



Hierarchical Self-Assembly of Hard Cube Derivatives

Journal:	<i>Soft Matter</i>
Manuscript ID	SM-ART-12-2018-002619.R1
Article Type:	Paper
Date Submitted by the Author:	18-Mar-2019
Complete List of Authors:	Harper, Eric; University of Michigan, Materials Science & Engineering Waters, Brendon; University of Michigan, Chemical Engineering Glotzer, Sharon; University of Michigan, Chemical Engineering



Soft Matter

ARTICLE

Hierarchical Self-Assembly of Hard Cube Derivatives

Eric S. Harper^a, Brendon Waters^b and Sharon C. Glotzer^{a,b,c,d}Received 27th December 2018,
Accepted 00th xxxxx 20xx

DOI: 10.1039/x0xx00000x

www.rsc.org/

Hierarchical, self-assembled structures are ordered on multiple scales, and formed by objects comprised of even smaller elements. Such structures are widely reported for nanoparticles, macromolecules, and peptides, and even in entropy-driven hard particle assembly hierarchical colloidal crystals have been reported. Here we consider the hierarchical self-assembly of a cubic colloidal crystal from congruent hard cube derivatives, and investigate how various ways of slicing and dicing a cube can affect the ability of the pieces to entropically re-assemble the initial colloidal crystal formed from perfect cubes. We present design rules that support heuristics reported for different systems, and present evidence for a previously unreported cubatic phase from 2:1 rectangular prisms.

Introduction

In hard particle self-assembly, particle shape has a profound effect on the colloidal crystal phases possible^{1–5} because shape affects the strength and directionality of the entropic bonds that emerge upon crowding^{6–11}. A variety of crystal structures have been predicted and experimentally realized for entropy-driven self-assembly^{1,12–17}, including complex structures such as quasicrystals¹⁸. Upon crowding, emergent, directional entropic forces (DEFs) produce local motifs^{7–10} – arrangements of small groups of particles – just as enthalpic forces do. These motifs can be either compatible or incompatible with the minimum free energy structure, producing a liquid crystal, plastic crystal, or crystal in the case of the former, or a glass in the case of the latter^{1,19}.

There are now numerous reported examples of entropy-driven self-assembly resulting in a hierarchically ordered colloidal crystal. Among the most complex are the dodecagonal quasicrystal formed from hard tetrahedra; this structure can be decomposed into identical, interlocking motifs of many tetrahedra. Even simpler are colloidal crystals where objects of low symmetry combine to create an object of higher symmetry that serves as the fundamental building unit in the crystal. For example, square pyramids derived from cubes¹ self-assemble a cubic crystal lattice (forming so-called “supercubes”), hard hemispherical caps self-assemble into a “double FCC” crystal structure²⁰, lock-and-key particles form superlattice

structures²¹, and aspect ratio 2:1 rectangular prisms, which pair to form a cube, self-assemble a cubic crystal^{22,23}. In fact, the phase behaviour of these rectangular prisms is rich, having stable reported smectic and columnar intermediate phases²³, while related rectangular prisms and other “thin” shapes such as cut spheres and cylinders^{24,25} also self-assemble a cubatic phase; the existence of the cubatic phase, in which there is long range orientational order without any translational order, is currently not known for 2:1 aspect ratio rectangular prisms. This assembly behaviour is in contrast to the two-dimensional (2D) analogue of the rectangular prisms, 2:1 rectangles, which self-assemble a random domino (parquet) phase^{23,26–28}, or the related right-isosceles triangles that do not self-assemble an ordered phase⁹. The final self-assembled phase of the rectangles and triangles may be controlled *via* allophilic patterning, using the directional entropic forces arising from particle shape upon crowding to direct the self-assembly of the desired square tiling. This leads us to the question: what shape features permit or inhibit hierarchical, entropy-driven self-assembly in a hard particle system of hard cube derivatives?

Here we investigate the self-assembly behaviour of a family of congruent hard cube^{14,29–31} derivatives obtained by decomposing a cube into identical pieces (shown in Figure). These include 2:1 rectangular prisms (RP) and right-isosceles triangular prisms (TP) (both 3D analogues of 2D polygons considered previously⁹); rhomb-faced prisms (RFP) and hexagonal-faced prisms (HFP), created by cutting a cube in two through its centre, forming distinct cut-faces; and two types of supercube shapes, “S3” and the square pyramid¹ “S6”, which require three and six pieces, respectively, to form a cube. We report the self-assembly behaviour of each shape obtained from Hard Particle Monte Carlo (HPMC³²) simulations, including evidence for a previously unreported cubatic phase for 2:1 rectangular prisms. We consider the geometric motifs formed by cubic assemblies of particles in the high-density fluid phase

^a Department of Materials Science and Engineering, University of Michigan, Ann Arbor, Michigan 48109, USA.

^b Department of Physics, University of Michigan, Ann Arbor, Michigan, 48109, USA.

^c Department of Chemical Engineering, University of Michigan, Ann Arbor, Michigan, 48109, USA.

^d Biointerfaces Institute, University of Michigan, Ann Arbor, Michigan 48109, USA.

† Corresponding author: sglotzer@umich.edu.

Electronic Supplementary Information (ESI) available: [details of any supplementary information available should be included here]. See DOI: 10.1039/x0xx00000x

prior to crystallization and demonstrate what makes a shape effective at hierarchically assembling a cubic crystal.

Methods

We simulated systems of $N=1000$ cubes ($N_{RP}=N_{TP}=N_{RFP}=N_{HFP}=2000$; $N_{S3}=3000$; $N_{S6}=6000$) in the *NPT* thermodynamic ensemble with the HOOMD-Blue^{33–36} simulation software, utilizing the HPMC³² plugin for hard particle MC simulation. These system sizes were chosen because we have learned in practice that systems on that scale are large enough to avoid finite size effects and small enough to observe bulk self-assembly behaviour over reasonable waiting times, except in extraordinary cases where the unit cells are very large. Systems were initialized and equilibrated in the fluid phase at low packing density $\phi = 0.2$, and then equilibrated and crystallized at the target pressure $P^* = \beta P \sigma^3$ where $\sigma^3 = V_{\text{cube}} = 1.0$. We allowed systems to equilibrate (as determined by volume oscillations) before computing any quantities. To allow

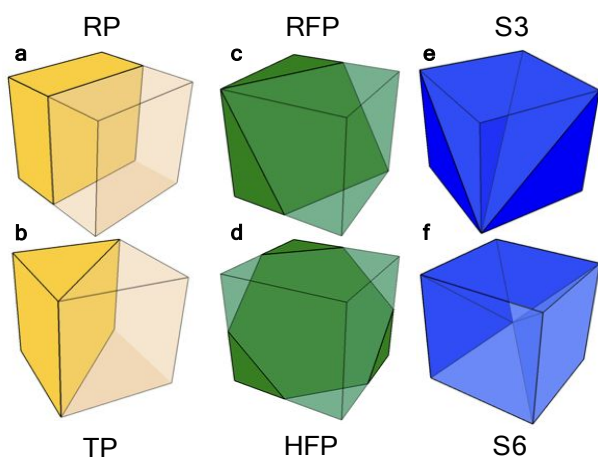


Figure 1 Illustration of shapes studied in this paper: **a** rectangular prisms (RP); **b** right-isosceles triangular prisms (TP); **c** rhomb-faced polyhedra (RFP); **d** hexagonal-faced polyhedra (HFP); **e** 3 piece supercubes (S3); and **f** 6 piece supercubes (S6). The cube formed by the assembled shapes is rendered with one (or more) of the pieces transparent to better show the faces that touch in the assembled cube. These decompositions are chosen as they yield congruent shapes (each shape arising from decomposing the cube is the same). RP and S6 have been previously studied.

these systems sufficient time to self-assemble, they were run for at least $3e8$ MC sweeps. The self-assembled structure was identified by calculating diffraction patterns¹, bond-order diagrams¹, and the cubic order parameter³⁷, as well as by visual inspection.

To analyse particle pair motifs, the local geometric configuration of a particle pair must be computed. The position and orientation of a particle is given by a vector and a quaternion, (\vec{v}_i, \vec{q}_i) . We can express the vector connecting two particles (i, j) in a local coordinate system of a particle by using the inverse quaternion operation: $\vec{r}_{ij} = \vec{r}_j - \vec{r}_i$, $\vec{r}_{ij, \text{local}} = \vec{q}_i^* \cdot \vec{r}_{ij} \cdot \vec{q}_i$. We can also express the orientation of the paired particle j relative to particle i using the quaternion operation with a unit vector $\hat{u}_{ij} = \vec{q}_i^* \cdot \vec{q}_j \cdot (0,0,1) \cdot \vec{q}_j^* \cdot \vec{q}_i$. By computing the vector

pair $\hat{r}_{ij}, \hat{u}_{ij}$ for a pair of particles, we obtain four unit vectors that may be combined to analyze preferred geometric motifs present in the system: $(\hat{r}_{ij}, \hat{u}_{ij}, \hat{r}_{ji}, \hat{u}_{ji})$. Combined with the length of the interparticle vector, $|\vec{r}_{ij, \text{local}}|$, we obtain a vector in 13-dimensional space.

Although each of these vectors may be visualized individually, visualizing multiple vectors at a time proves problematic as we cannot natively visualize nor intuitively understand > 3 dimensions. Instead, we employ a dimensionality-reduction technique known as t-Stochastic Neighbour Embedding (t-SNE)^{38–40}. This technique embeds a higher-dimensional distribution in a lower dimension, in this case reducing 13 dimensions to 2 (see Supplemental Information *t-Stochastic Neighborhood Embedding*, Figure 1 for more information). t-SNE accomplishes this by keeping points that are close in the

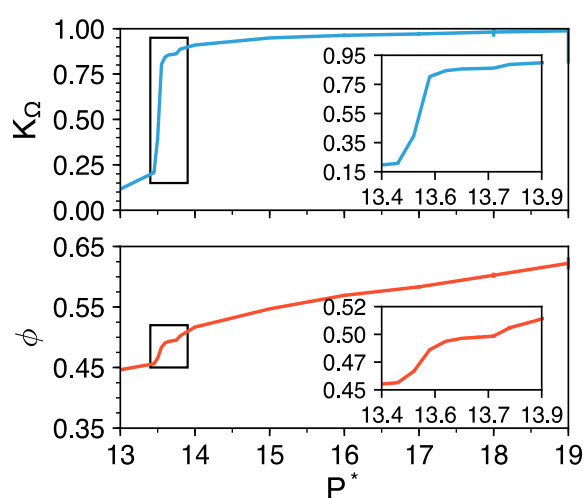


Figure 2 Cubatic order parameter, K_{Ω} vs. pressure P^* (top panel), and the equation of state (bottom panel) for 2:1 rectangular prisms, showing the existence of a previously unreported cubatic phase, evidenced by the simultaneous increase in both K_{Ω} and ϕ at $P^* \approx 13.5$. The slight increase in K_{Ω} with an increase in ϕ at $P^* \approx 13.8$ shows the transition from the cubatic phase to a smectic phase. Insets highlight the fluid-cubatic-smectic phase transition. See Figure 1 for images of the cubatic phase.

higher dimensional space also close in the reduced dimensional space. We performed t-SNE analysis on a set of 8000 randomly sampled pair geometry vectors from 10 independent simulation trajectory frames for each cube decomposition at the highest observed equilibrium fluid pressure (that is, just below the crystallization pressure).

We then clustered similar points in this lower dimensional space via Gaussian mixture methods^{40–42}, allowing us to identify pair motifs preferred by the system. This method provides an alternative to both the potential of mean force and torque^{7,8,10} and explicit geometric definitions of pairing⁹ to identify particular local motifs present in the dense fluid phase. We then categorized these motifs based on their contribution to the final ordering of the system: cut-face pairs (faces that form from the correctly cut pair), square-face pairs (faces that form from the original square faces of the cube), compatible motifs (motifs that do not have congruent faces pairing, but nonetheless contribute to the final crystal structure, and are thus “native”

motifs), and competing motifs (motifs that are not found in the final crystal and thus compete with the desired self-assembly (non-native motifs)). This analysis provides insight into the self-assembly pathways for the different shapes. By analysing these motifs in the context of the final self-assembled crystal, we can understand the self-assembly behaviour of these systems in conjunction with known hierarchical design rules⁴³.

Results and Discussion

The pressure dependence of the cubatic order parameter K_{Ω} and the equation of state for RP is shown in Figure . We observe a transition to an intermediate phase between the fluid phase ($P^* < 13.5$) and a previously reported smectic phase ($P^* < 13.8$). We identify this intermediate phase as a cubatic phase, evidenced by the increase in K_{Ω} in this region of the equation of state. The difference in the cubatic and smectic phases is shown in Figure , where the peaks in the bond-order diagram (Figure b) show local cubatic ordering and the diffraction pattern (Figure c) shows no long-range translational ordering for the cubatic phase, while these quantities in the smectic phase (Figure e,f) show clear development of layers. This quantities demonstrate evidence for a previously unreported cubatic phase for 2:1 aspect ratio rectangular prisms; it was previously reported to not assemble such a phase²³. At higher pressures, we observe a cubic crystal (Figure g-i).

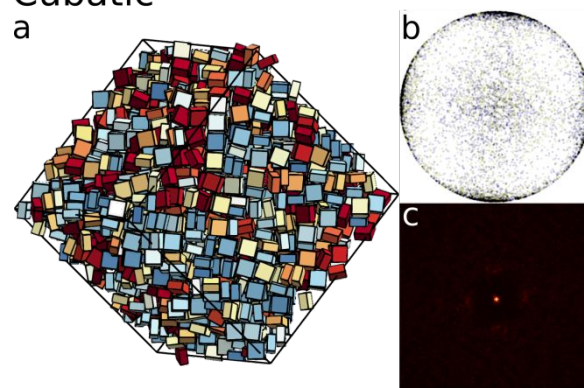
The square-pyramid supercube (S6) was previously reported to self-assemble into a cubic crystal¹. We also observe this self-assembly (Figure); however, the process is prone to multiple nucleation sites, making the self-assembly of a single crystal difficult. To understand why this is the case, we employ the t-SNE analysis of the pair geometry vectors, shown in Figure . We observe four major clusters of pair configurations, belonging to three classes of motifs: triangle-triangle, square-square, and square triangle.

Analyzing the population fraction of the S6 motifs (Figure), we find the cut-face motif (Figure , triangle-triangle green motif) $\approx 49\%$, making it the predominant motif. The frequency of this motif is surprising to us because we would expect that the smallest face of the S6 shape (the triangular face) to be associated with the lowest DEFs and thus have a lower frequency of self-assembly in the high-density fluid phase; in contrast, the larger square faces that we would expect to be associated with higher DEFs align only 21% of the time. We conclude the high assembly propensity is a result of the larger number of ways for triangular faces to pair, rather than simply the size of the faces. The high population fraction of motifs associated with the cubic phase also explains the observation of multiple crystal grains originating from multiple nucleation sites in the S6 system (note the two cubic crystal grains present in the assembly shown in Figure).

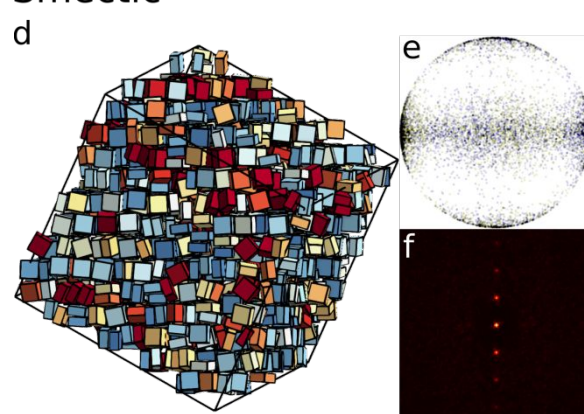
We performed the same t-SNE dimensionality reduction on the remaining shapes: HFP, RFP, TP, and the S3 supercube (see

Supplemental Figures 2-4 for the t-SNE figures). Of these

Cubatic



Smectic



Cubic

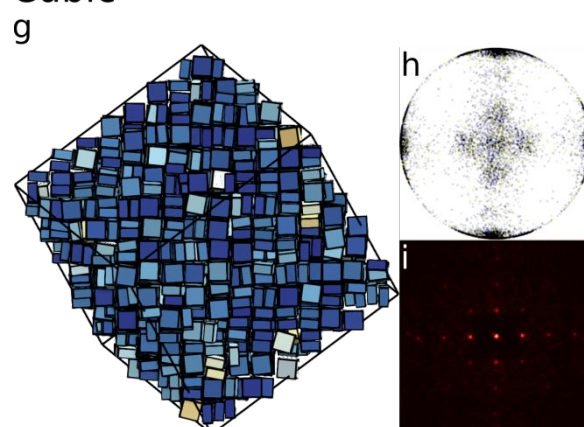


Figure 3 Comparison of the cubatic ($P^* = 13.65$) a-c, smectic ($P^* = 14.0$) d-f, and cubic ($P^* = 21.0$) g-i phases. The bond-order diagrams (b, e, h) show order with the six sides of a cube, with additional equatorial ordering in the smectic phase (e). Note the disappearance of the equatorial band from the smectic to cubic phase. No long-range translational order is present in the cubatic phase as measured by the diffraction pattern (c), while the layering is clearly present in the smectic phase (f), and the cubic order is present in the cubic phase (i).

shapes, only the S3 shape fails to self-assemble an ordered phase (see Figure d). Considering the pair motifs observed for the S3 shape (Figure), we see that more than half of the pairs are misaligned and incompatible with the target cubic crystal. This incompatibility makes any self-assembly prohibitively difficult^{19,43}.

The polyhedral shapes HFP and RFP both successfully self-assemble the cubic crystal (Figure a,b). Like S6, HFP forms only “native” motifs that directly contribute to the cubic crystal (Figure a) and does not form other motifs. This behaviour is a result of the symmetry of the HFP: the cut-face has three equivalent alignments, and each of the large faces that result from the original square faces on the cube are congruent, thereby exhibiting no alignment preference. In contrast, RFP forms not only native motifs but also other contributing motifs (Figure b), due to its incongruent faces: the bottom square face is different from the other large faces that result from the original square face, and those two faces are not congruent. Additionally, the cut-face to cut-face motif has only one correct alignment; while the rhomb itself has 2-fold symmetry, the pair assembly is only 1-fold symmetric. This results in the smaller population of the cut-face motif and the larger population of misalignment in RFP relative to HFP. However, because the final crystal structure is compatible with the contributing motifs, both HFP and RFP successfully self-assemble the cubic crystal structure.

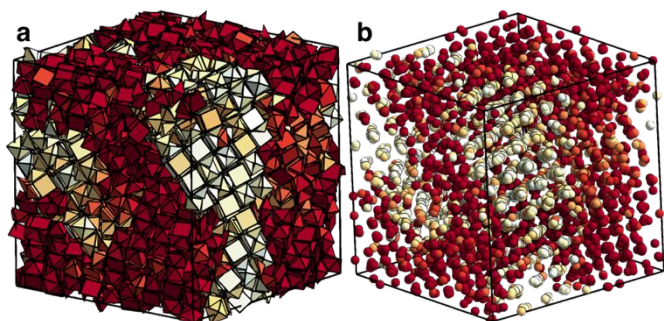


Figure 4 View of the self-assembled supercube structure of the S6 shape at a pressure of $P^* = 53.0$, showing two different crystal grains (red and off-white). a shows the actual particles, while b shows the particle centre-of-mass shifted to the tip, showing the cubic crystalline structure.

The right-isosceles triangular prism also manages to self-assemble the cubic crystal phase (Figure c). From the assembly itself, as well as from the bond-order diagram and diffraction pattern, the quality of the assembly for the TP is not as good as for the HFP and RFP. In contrast to the 2D right-isosceles triangle⁹, the additional dimension adds the additional contributing motifs that drive the system to an ordered assembly; the total population of motifs leading to or compatible with the final assembly is $f \approx 0.6$ (Figure).

Quantification of these motifs is based on previous investigation into assembly pathway engineering⁴³. Ref. 43 suggested that when local motifs form and compete with the target structure, the assembly of the target structure will be hindered or even prevented. Our observations reflect and reinforce this conclusion, as the only shape that did not self-assemble the target crystal (S3) has a fluid phase dominated by competing motifs¹⁹ (see Figure). These observations and analysis may be summarized in the following design rules:

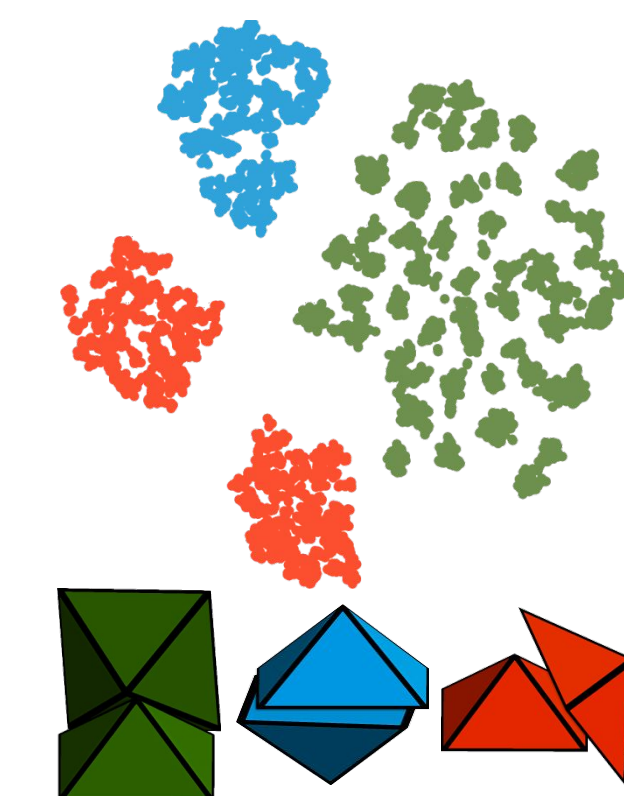


Figure 5 t-SNE analysis and classification of the S6 shape at $P^* = 50.0$. This shape exhibits only three of the four possible geometric motifs: triangle-triangle (blue), square-square (red), and triangle-square (green); this shape does not form other motifs which contribute to the simple cubic crystal.

1. Shapes should maximize the number of correct ways to assemble compatible motifs, and minimize the number of ways to incorrectly assemble incompatible motifs.
2. Shapes should possess “selectivity”; individual particle faces should be different enough to prevent local motif “confusion.”

Both the HFP and S6 shapes demonstrate the synergy of these rules. Both shapes avoid forming compatible motifs – motifs that result from non-matching faces but are allowed in the final

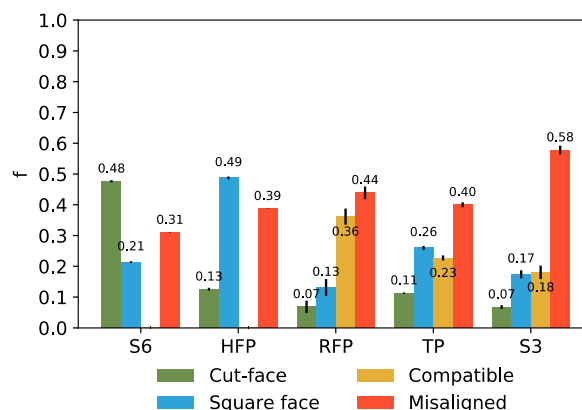


Figure 6 Comparison of the fraction of pair motifs found in the dense fluid phase for S6, HFP, RFP, TP, and S3 shapes. Note that S6 and HFP do not form other contributing motifs, and that the S3 shape is not observed to self-assemble the cubic crystal lattice.

crystal. In contrast, the compatible motifs arising in both RFP and TP shapes allow for multiple intermediate motifs to assemble. The S3 shape, and its failure to self-assemble, exemplifies these design rules. While faces resulting from the original square faces are congruent, allowing for multiple chances for correct assembly, these faces are similar enough to the cut triangle faces to introduce motif confusion, introducing competition between compatible and incompatible motifs. This competition results in a decreased ability to self-assemble the final correct structure. Additionally, the cut triangle faces are not congruent, but are similar in shape, again introducing confusion⁴⁴ and ultimately competition. The interplay of these design rules will also impact hierarchical self-assembly in polydisperse systems^{45,46}, allowing the system to self-assemble the target phase as long as the polydispersity does not introduce local motifs⁴⁴ that compete with the original structure.

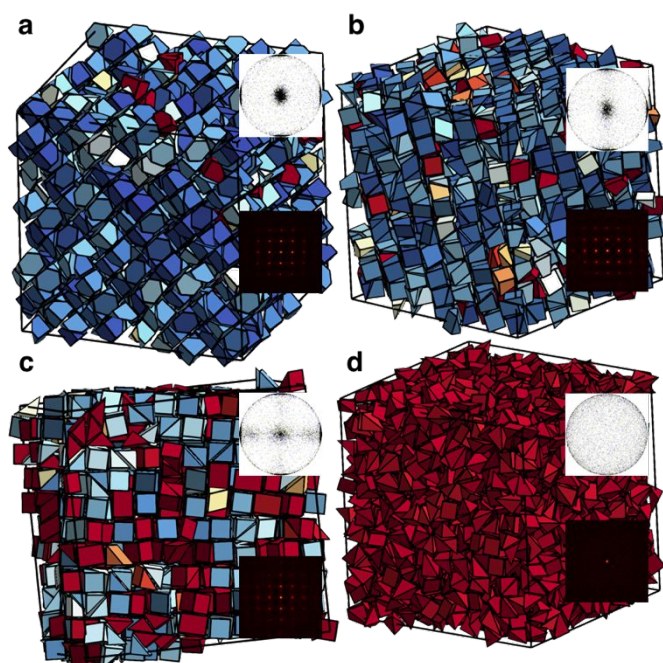


Figure 7 Equilibrium self-assemblies colored by cubatic order parameter, with inset bond-order diagrams (top) and diffraction patterns (bottom) of **a** HFP at $P^* = 21.0$, **b** RFP at $P^* = 24.0$, **c** TP at $P^* = 18.0$, and **d** S3 at $P^* = 36.0$. Only the S3 shape fails to self-assemble an ordered cubic crystal.

These design rules agree with the results of 2D self-assembly of “jig-saw” rectangles and triangles⁹. The saw-tooth patterns introduced on matching shape edges promoted the assembly of compatible motifs and inhibited the assembly of incompatible motifs, provided the saw-tooth pattern had a sufficiently large wavelength relative to the edge length. This so-called allophilic patterning was capable of overcoming the DEFs that prevent the entropy-driven self-assembly of right-isosceles triangles, successfully self-assembling the square lattice. The use of allophilic patterning should be capable of altering the DEFs present in the S3 system, and should be considered for further investigation.

Conclusions

We showed that different “cube slices” successfully assemble the parent cube, and self-assemble a hierarchical simple cubic crystal in most cases. We reported evidence for a cubatic phase in systems of 2:1 aspect ratio rectangular prisms, and reproduced the self-assembly of hard square pyramids into a so-called “supercube” cubic crystal structure. In our investigation of all six cube-derivative shapes, we quantified the observed pair motifs and related them to the geometric features of the self-assembled crystal. By categorizing these motifs into classes compatible with or competing with successful self-assembly, we provided insight into desirable and undesirable shape features to be considered in building block design and selection. Even in the presence of intrinsic attractive interactions, entropic interactions arising from particle shape can contribute to – or interfere with – self-assembly, and should be considered in building block design and selection.

This investigation did not observe local motifs that could lead to the self-assembly of multiple possible crystal structures, for example, square pyramids that may either self-assemble into octahedra or rectangular pyramids. Future research into assembly engineering of such “pluripotent” particles should be considered. Use of the t-SNE dimensionality reduction technique facilitated investigation of the pair motifs. Previous studies utilized the potential of mean force and torque (PMFT)^{8,10} to understand the preferred pair motifs and quantify the entropic driving force underlying their formation. In the systems we studied, a six-dimensional PMFT would be required to properly account for the different pair motifs. Our current software^{47,48} does not yet perform this complex calculation, requiring additional development of these techniques. The resulting PMFT would provide additional insight into the effective driving force to form these motifs, as well as the topology of the free-energy landscape, allowing shapes more effective at hierarchical self-assembly to be designed.

Conflicts of interest

There are no conflicts to declare.

Acknowledgements

This material is based upon work supported by the Center for Photonic and Multiscale Nanomaterials (C-PHOM) funded by the National Science Foundation Materials Research Science and Engineering Center program DMR 1120923. E.S.H. was also supported by a National Science Foundation DGE 0903629 OpenData IGERT Fellowship. Undergraduate student B.W. was supported by supported by a Simons Investigator award from the Simons Foundation to Sharon Glotzer. This work used the Extreme Science and Engineering Discovery Environment (XSEDE), which is supported by National Science Foundation grant number ACI-1053575; XSEDE award DMR 140129. Additional computational resources and services were supported by Advanced Research Computing at the University

of Michigan, Ann Arbor. We acknowledge the contributions of Jeffrey Wan, a summer student in the NSF MRSEC – funded C-PHOM high school program, and Matthew Spellings regarding the use of the t-SNE, Gaussian mixture methods, and the merging of Gaussian regions for the quantification of geometric pair motifs. Figures in this work produced with Matplotlib⁴⁹. Data analysis in this work made possible by Freud^{47,48} and the Python scientific computing stack: NumPy, SciPy, IPython, and Scikit Learn^{50–55}.

References

- P. F. Damasceno, M. Engel and S. C. Glotzer, *Science*, 2012, **337**, 453–457.
- K. P. Velikov, T. van Dillen, A. Polman and A. van Blaaderen, *Appl. Phys. Lett.*, 2002, **81**, 838–840.
- L. Bo, D. Zhou and Y. Han, *Nat. Rev. Mater.*, 2016, **1**, 1–13.
- R. J. Macfarlane, B. Lee, M. R. Jones, N. Harris, G. C. Schatz and C. a Mirkin, *Science*, 2011, **334**, 204–8.
- F. Li, D. P. Josephson and A. Stein, *Angew. Chem., Int. Ed.*, 2011, **50**, 360–388.
- P. F. Damasceno, M. Engel and S. C. Glotzer, *ACS Nano*, 2012, **6**, 609–614.
- G. van Anders, N. K. Ahmed, R. Smith, M. Engel and S. C. Glotzer, *ACS Nano*, 2014, **8**, 931–40.
- G. van Anders, D. Klotsa, N. K. Ahmed, M. Engel and S. C. Glotzer, *Proc. Natl. Acad. Sci.*, 2014, **111**, E4812–E4821.
- E. S. Harper, R. L. Marson, J. A. Anderson, G. van Anders and S. C. Glotzer, *Soft Matter*, 2015, **11**, 7250–7256.
- E. S. Harper, G. van Anders and S. C. Glotzer, *Proc. Nat. Acad. Sci. USA*, 2018, Preprint.
- E. S. Harper, J. Anderson, G. Van Anders and S. C. Glotzer, 2019, Preprint.
- K. L. Young, M. L. Personick, M. Engel, P. F. Damasceno, S. N. Barnaby, R. Bleher, T. Li, S. C. Glotzer, B. Lee and C. A. Mirkin, *Angew. Chem. Int. Ed. Engl.*, 2013, **52**, 13980–4.
- M. D. Eldridge, P. A. Madden and D. Frenkel, *Nature*, 1993, **365**, 35–37.
- A. P. Gantapara, J. de Graaf, R. van Roij and M. Dijkstra, *J. Chem. Phys.*, 2015, **142**, 54904.
- U. Agarwal and F. A. Escobedo, *Nat. Mater.*, 2011, **10**, 230–235.
- J. M. Meijer, A. Pal, S. Ouhajji, H. N. W. Lekkerkerker, A. P. Philipse and A. V. Petukhov, *Nat. Commun.*, 2017, **8**, 1–8.
- D. El Masri, T. Vissers, S. Badaire, J. C. P. Stiefelwagen, H. R. Vutukuri, P. Helfferich, T. H. Zhang, W. K. Kegel, A. Imhof and A. Van Blaaderen, *Soft Matter*, 2012, **8**, 6979–6990.
- A. Haji-Akbari, M. Engel, A. S. Keys, X. Zheng, R. G. Petschek, P. Palfy-Muhoray and S. C. Glotzer, *Nature*, 2009, **462**, 773–777.
- E. G. Teich, G. van Anders and S. C. Glotzer, *Prep.*, 2017, 1–22.
- M. Marechal, R. J. Kortschot, A. F. Demirörs, A. Imhof and M. Dijkstra, *Nano Lett.*, 2010, **10**, 1907–1911.
- N. K. Ahmed, G. van Anders, E. R. Chen and S. C. Glotzer, *arXiv e-prints*, 2015, arXiv:1501.03130.
- B. S. John, C. Juhlin and F. A. Escobedo, *J. Chem. Phys.*, 2008, **128**, 44909.
- B. S. John and F. A. Escobedo, *J. Phys. Chem. B*, 2005, **109**, 23008–15.
- R. Blaak, D. Frenkel and B. M. Mulder, *J. Chem. Phys.*, 1999, **110**, 11652–11659.
- P. D. Duncan, M. Dennison, A. J. Masters and M. R. Wilson, *Phys. Rev. E - Stat. Nonlinear, Soft Matter Phys.*, 2009, **79**, 1–11.
- A. Donev, J. Burton, F. H. F. Stillinger and S. Torquato, *Phys. Rev. B*, 2006, **73**, 054109.
- D. A. Triplett and K. A. Fichtorn, *J. Chem. Phys.*, 2010, **133**, 144910.
- D. A. Triplett and K. A. Fichtorn, *Phys. Rev. E*, 2008, **77**, 11707.
- L. Rossi, S. Sacanna, W. T. M. Irvine, P. M. Chaikin, D. J. Pine and A. P. Philipse, *Soft Matter*, 2011, **7**, 4139–4142.
- F. Smalenburg, L. Filion, M. Marechal and M. Dijkstra, *Proc. Natl. Acad. Sci.*, 2012, **109**, 17886–17890.
- R. Ni, A. P. Gantapara, J. de Graaf, R. van Roij and M. Dijkstra, *Soft Matter*, 2012, **8**, 8826.
- J. A. Anderson, M. Eric Irgang and S. C. Glotzer, *Comput. Phys. Commun.*, 2016, **204**, 21–30.
- J. A. Anderson, HOOMD-blue, <http://codeblue.umich.edu/hoomd-blue>.
- J. a. Anderson, C. D. Lorenz and a. Travesset, *J. Comput. Phys.*, 2008, **227**, 5342–5359.
- J. Glaser, T. D. Nguyen, J. A. Anderson, P. Lui, F. Spiga, J. A. Millan, D. C. Morse and S. C. Glotzer, *Comput. Phys. Commun.*, 2015, **192**, 97–107.
- M. P. Howard, J. A. Anderson, A. Nikoubashman, S. C. Glotzer and A. Z. Panagiotopoulos, *Comput. Phys. Commun.*, 2016, **203**, 45–52.
- A. Haji-Akbari and S. C. Glotzer, *J. Phys. A Math. Theor.*, 2015, **48**, 1–19.
- L. Van Der Maaten and G. Hinton, *J. Mach. Learn. Res.*, 2017, **620**, 267–284.
- L. Van Der Maaten, *J. Mach. Learn. Res.*, 2014, **15**, 3221–3245.
- M. Spellings and S. C. Glotzer, *AIChE J.*, 2018, **64**, 2198–2206.
- A. P. Dempster, N. M. Laird and D. B. Rubin, *J. R. Stat. Soc. Ser. B Methodol.*, 1977, **39**, 1–38.
- J. P. Baudry, A. E. Raferty, Celeux Gilles, Lo Kenneth and R. Gottardo, *J. Comput. Graph. Stat.*, 2010, **19**, 332–353.
- E. Jankowski and S. C. Glotzer, *Soft Matter*, 2012, **8**, 2852.
- E. G. Teich, G. van Anders and S. C. Glotzer, *Nat. Commun.*, DOI:10.1038/s41467-018-07977-2.
- C. L. Phillips and S. C. Glotzer, *J. Chem. Phys.*, DOI:10.1063/1.4748817.
- Y. Xia, T. D. Nguyen, M. Yang, B. Lee, A. Santos, P. Podsiadlo, Z. Tang, S. C. Glotzer and N. A. Kotov, *Nat. Nanotechnol.*, 2011, **6**, 580.
- E. S. Harper, V. Ramasubramani, B. D. Dice, M. P. Spellings, J. A. Anderson and S. C. Glotzer, *Comput. Phys. Commun.*, 2019, In Preparation.
- E. S. Harper, M. P. Spellings, J. A. Anderson and S. C. Glotzer, Freud: A Software Suite for High-Throughput

- Analysis, <https://bitbucket.org/glotzer/freud>.
- 49 J. D. Hunter, *Comput. Sci. Eng.*, 2007, **9**, 90–95.
- 50 E. Jones, T. Oliphant, P. Peterson and others, SciPy: Open source scientific tools for Python, <http://www.scipy.org/>.
- 51 T. E. Oliphant, *Comput. Sci. Eng.*, 2007, **9**, 10–20.
- 52 K. J. Millman and M. Aivazis, *Comput. Sci. Eng.*, 2011, **13**, 9–12.
- 53 S. van der Walt, S. C. Colbert and G. Varoquaux, *Comput. Sci. Eng.*, 2011, **13**, 22–30.
- 54 F. Pérez and B. E. Granger, *Comput. Sci. Eng.*, 2007, **9**, 21–29.
- 55 F. Pedregosa, G. Varoquaux, A. Gramfort, V. Michel, B. Thirion, O. Grisel, M. Blondel, P. Prettenhofer, R. Weiss, V. Dubourg, J. Vanderplas, A. Passos, D. Cournapeau, M. Brucher, M. Perrot and E. Duchesnay, *J. Mach. Learn. Res.*, 2011, **12**, 2825–2830.

